PDO-driven interdecadal variability of snowfall over the Karakoram and Western Himalaya

Authors: Priya Bharati[1], Pranab Deb[1], Kieran M. R. Hunt[2,3]

1 Centre for Ocean, River, Atmosphere and Land Sciences (CORAL), Indian Institute of Technology Kharagpur, Kharagpur, India

2 Department of Meteorology, University of Reading, Reading, UK

3 National Centre for Atmospheric Science, University of Reading, UK

***Correspondence to*: pranab@coral.iitkgp.ac.in**

Abstract:

Our study reveals that the negative phase of the Pacific Decadal Oscillation (PDO-) leads to increased winter (DJF) snowfall in the Karakoram and Western Himalayas (KH) from 1940 to 2022. Interdecadal variations in DJF snowfall during the PDO- are attributed to deep convection and adiabatic cooling near the tropopause in both the northwest Pacific and KH region. Additionally, a wave-like pattern characterized by a trough (anomalous cyclone) north of KH and a ridge (anomalous Tibetan Plateau anticyclone) east of KH in the upper atmosphere, along the northward shift of the DJF Subtropical Jet (STJ) was observed. A strong positive correlation between DJF STJ strength and DJF snowfall in KH as well as a significant negative correlation between DJF STJ strength and DJF PDO, suggests a wave response over KH to the direct forcing over the northwest Pacific Ocean. The intensified STJ across KH results in higher frequency of Western disturbances, leading to anomalous moisture convergence and increased DJF precipitation in the region during the PDO-. These findings hold significant implications for the decadal predictability of winter snowfall in KH by the various phases of PDO.

1) Introduction:

Glaciers in the Karakoram and Western Himalaya (KH) exhibit unique stability compared to other alpine glaciers (known as the ‘Karakoram Anomaly’; Hewitt, 2005; Kaab et al., 2012; Gardelle et al., 2013; Kapnick et al., 2014; Forsythe et al., 2017; de Kok et al., 2018; Farinotti et al., 2020; HIMAP, 2020). Winter snowfall plays a significant role in preserving the local snowpack and sustaining the glacial mass balance at higher elevations (Tahir et al., 2011; Bolch et al., 2012; Ridley et al., 2013; Cannon et al., 2015; Dimri et al., 2015), and controls almost 60% of the variability in glacier mass balance in the KH region (Kumar et al., 2019). The decline in average and minimum summer temperatures, along with significant increases in winter, summer, and annual precipitation, have been proposed as crucial factors influencing the stable glacier budget of the KH in recent decades (Archer and Fowler, 2006; Forsythe et al., 2017).

The KH receives around 50% of its annual precipitation as snowfall from western disturbances (WDs) (Lang and Barros, 2004; Barros et al., 2006; Bookhagen and Burbank, 2010; Hunt et al., 2024). Furthermore, WDs account for more than 65% of all winter snowfall and nearly 53% of total winter precipitation in the KH (Javed et al., 2022). However, using a less conservative method, Midhuna et al. (2020) found that WDs account for about 80% of winter precipitation in KH. WDs

are upper-level troughs in the subtropical westerly jet (STJ), which grow via baroclinic instability (Norris et al., 2015; Cannon et al., 2017; Hunt et al., 2018). Strong WDs are associated with deep uplift to the east of their centre and drive moist lower-tropospheric southwesterlies from the Arabian Sea (Dimri and Dash, 2012; Hunt et al., 2018), resulting in heavy precipitation along the foothills and mountains of KH region (Baudouin et al., 2020). The snowfall from WDs in the KH is heavily influenced by the complex topography of the region, as well as by synoptic and mesoscale factors (Cannon et al., 2015; Norris et al., 2015, 2017, 2018). Subsequent snowmelt in the following spring and summer seasons and associated runoff serve as major sources of downstream river flow and provide relief from drought to populations that are vulnerable to water stress (Bolch et al., 2012; Hewitt et al., 2014; Rana et al., 2019; Pritchard et al., 2019).

However, the main climatic drivers affecting seasonal precipitation, and hence glacial mass balance in the region are only partially understood (Cannon et al., 2015). WD activity during winter season over the KH has been reported to be influenced by several global climate forcings such as North Atlantic Oscillation/Arctic Oscillation (Yadav et al., 2009; Syed et al., 2010; Filippi et al., 2014; Basu et al., 2017; Midhuna and Dimri, 2019; Hunt and Zaz, 2022), El Niño–Southern Oscillation (ENSO) (Yadav et al., 2010; Dimri, 2013; Kar and Rana, 2014; Cannon et al., 2017; Kamil et al., 2019; Rana et al., 2019; Bharati et al., 2024), Polar/Eurasian Pattern and Siberian High (Wu and Wang, 2002; Cannon et al., 2014), Madden–Julian Oscillation (Barlow et al., 2005; Cannon et al., 2017) and Indian Ocean Dipole (IOD) (Yadav et al., 2007; Hoell et al., 2013) on intraseasonal and interannual timescales. In particular, the ENSO exerts the strongest influence on the interannual variability of winter precipitation in KH (Rana et al., 2019). One of the key aspects of ENSO teleconnection to Indian Himalayas is the southward shift in the latitude of the winter STJ over the KH during the positive phase of ENSO (Cannon et al., 2014, 2017), which leads to heavier WD precipitation as their tracks move closer to their primary moisture source, the Arabian Sea (Bharati et al., 2024).

Precipitation gauges in the Himalayas are sparse and recognised as inadequate for accurately measuring snowfall (Anders et al., 2006; Rana et al., 2015). While satellite records of precipitation are available, they cover only a limited time frame, whereas our study requires long-term data to analyse the interdecadal variability of precipitation over the KH region. We currently have an 85-year-long reanalysis from ERA5, which has demonstrated a high degree of similarity in both the

quantity and variability of winter precipitation across all time scales when compared to observations and satellite data in the KH region (Baudouin et al., 2020). The long dataset from ERA5 is sufficient to examine the interdecadal variability of DJF snowfall over KH. The low-frequency modes of atmospheric variability such as the Pacific Decadal Oscillation (PDO), Inter-decadal Pacific Oscillation (IPO) (Mantua et al., 1998; Zhang et al., 1997; Power et al., 1999; Deser et al., 2004; Dai, 2013), and the Atlantic Multi-decadal Oscillation (AMO) (Enfield et al., 2001) are known to modulate the regional climate of the Northern Hemisphere over inter-decadal to multi-decadal timescales. Among these, the PDO is the dominant mode of SST oscillation in the North Pacific, influencing long-term precipitation patterns globally (Dettinger et al., 1998; Krishnamurthy, 2013, 2014; Wang et al., 2014; Dong and Dai, 2015; Yang et al., 2017; Wu and Mao, 2016; Qin et al., 2017; Aggarwal et al., 2023). For example, Indian monsoon rainfall and autumn precipitation in North Central China were found to have an inverse relationship with PDO (Krishnan and Sugi, 2003; Krishnamurthy, 2014; Qin et al., 2017). According to Aggarwal et al. (2023), the PDO has a stronger positive correlation with pre-monsoon precipitation in the northwest Himalayas compared to the ENSO and IOD, leading to a significant decrease in precipitation in recent decades. However, there remains a significant gap in our understanding of the PDO's impact on precipitation over the Himalayas during both monsoon and non-monsoon seasons.

The current study aims to address this knowledge gap by examining the modulation of the interdecadal variability of winter snowfall over KH by PDO. Our study aims to understand the potential influence of the PDO on the Karakoram anomaly, which deviates from the general climate change patterns observed in the KH region and other mountainous areas. The main objective of this study are: (1) To examine the spatial distribution of decadal snowfall in KH in different phases of PDO, (2) how the PDO adjusts global circulation patterns, leading to changes in the STJ, and (3) how these changes cause impact on a local scale over the KH through WDs and moisture transport.

2) Data and Methods:

2.1 Data

2.1.1) Meteorological data

The study uses meteorological data including geopotential height, zonal (u) and meridional wind (v) at 200 hPa level, vertically averaged temperature from 500 to 300 hPa level, vertically integrated

moisture flux (VIMF), vertically integrated moisture flux convergence (VIMFC), and global sea surface temperature (SST) obtained from the European Centre for Medium-Range Weather Forecasts (ECMWF) ERA5 reanalysis from 1940 to 2022. The jet latitude and strength are computed by 200 hPa zonal winds over the region (50° – 80°E, 10° – 60°N). The jet latitude is the mean of the latitudes with the largest value of u for each longitude and jet strength is the mean value of u along these latitudes. ERA5 data have global coverage at hourly frequency and a horizontal resolution of 0.25°.

2.1.2) Precipitation data

Precipitation in the KH is mainly observed through satellite derived and reanalysis products (Bosilovich et al., 2008; Joshi et al., 2012; Ménégoz et al., 2013; Palazzi et al., 2013; Rana et al., 2015; Kishore et al., 2016; Baudouin et al., 2020) due to limited and unreliable observations from ground stations in this complex topographical region (Anders et al., 2006; Bookhagen and Burbank 2006; Strangeways, 2010; Rana et al., 2015; Dahri et al., 2018). The ERA5 reanalysis has frequently been used for precipitation and snow in recent studies over the KH (Dahri et al., 2018; Baudouin et al., 2020; T. Singh et al., 2021) and neighbouring mountainous areas (Hu and Yuan, 2020; Li et al. 2021; Dollan et al., 2014). ERA5 closely matches the most reliable gridded measurements over KH in terms of amount, seasonality, and variability across all timescales during winter (Baudouin et al., 2020). However, the accuracy of precipitation datasets varies depending on the season in the region. We choose ERA5 due to its long period, allowing decadal-scale analysis where other datasets do not.

To assess the performance of ERA5 precipitation, we compared the ERA5 precipitation with various gridded precipitation datasets over the KH, including reanalysis datasets from ECMWF ERA5-land, Modern Era Retrospective-analysis for Research, Applications version 2 (MERRA2), and High Asia Refined analysis version 2 (HAR v2), as well as rain gauge, and satellite data from Climate Research Unit version 7 (CRU_TS v7), Global Precipitation Climatology Center version 2022 (GPCC), Global Precipitation Climatology Project version 3.2 (GPCP v3.2), Asian Precipitation - Highly-Resolved Observed Data Integration Towards Evaluation (APHRODITE MA_v1101), CPC-Merged Analysis of Precipitation (CMAP), Tropical Rainfall Measuring Mission (TRMM) Multi-satellite Precipitation Analysis (TMPA) 3B43, and Global Precipitation Measurement mission-Integrated Multi-satellite Retrievals version 7 (GPM_IMERG v7).

We computed the linear correlation coefficient between area-averaged precipitation over the KH region (cropped by the shapefile of the traditional boundaries of the Karakoram-Western and Central Himalaya; highlighted by a green box in Fig. 2a&b) in ERA5 and numerous other precipitation datasets. A strong correlation was seen between DJF ERA5 precipitation and rain-gauge-based precipitation products, including GPCC, GPCP, and CRU, with the exception of CMAP, which exhibited a correlation coefficient of 0.51 (Table 1). All reanalysis products, including ERA5 exhibit similar DJF precipitation variability as seen in observational and satellite datasets over the KH region. The variability of ERA5 precipitation in the KH region aligns closely with all available gridded datasets, despite the presence of biases in ERA5 precipitation across this region. Since most of DJF precipitation in KH occurs as snowfall (Fig. 1b), we utilize ERA5 snowfall data to examine the decadal variability of snowfall in the KH (73º – 78ºE, 33º – 38º N).

Table:1 Correlation coefficients of DJF precipitation based on monthly reanalysis, rain-gauge and satellite with ERA5 precipitation

	Name	**Time**	**Spatial resolution**	**Correlation with ERA5**	**Source**
Reanalysis	ERA5-land	1980-2022	0.25°	0.99	Hersbach et al., 2018
	HAR v2	1980-2020	0.1°	0.92	Wang et al., 2021
	MERRA2	1980-2022	0.5°	0.94	Gelaro et al., 2017
Rain-gauge based	CRU_TS v7	1980-2022	0.5°	0.84	Harris et al., 2014
	GPCC v2022	1980-2020	2.5°	0.89	Schneider et al., 2018
	GPCP	1998-2022	2.5°	0.89	Adler et al., 2016
	CMAP	1980-2022	2.5°	0.51	Xie and Arkin, 1997
	APHRODITE	1998-2015	0.25°	0.67	Yatagai et al., 2012

Satellite	GPM_IMERG v07	2000-2022	0.1°	0.86	Huffman et al., 2015
	TRMM 3B43	1998-2019	0.25°	0.85	Huffman et al., 2007

171

172 **2.1.2) PDO index**

173 The PDO index from the National Oceanic and Atmospheric Administration National Climate Data
174 Center (NOAA-NDC) (https://www.ncei.noaa.gov/access/monitoring/pdo/) is employed to describe
175 the interdecadal variability of the Pacific Ocean over the period 1940 to 2022.

176

177 **2.1.3) Western disturbance data**

178 WD statistics are computed from the WD track catalogue described in Hunt et al., (2018) and
179 Nischal et al., (2022), which is based on ERA5 reanalysis data that is spectrally truncated to T42 to
180 remove noise and small-scale structures. The tracking algorithm detects WDs by identifying upper-
181 tropospheric regions of positive relative vorticity averaged between 450 hPa and 300 hPa, with the
182 locations of candidate WDs identified as centroids of these regions. The candidate WDs are then
183 further refined by only accepting those: 1) whose locations are linked through time to form tracks
184 that generally follow the westerly steering winds associated with the STJ, 2) that persist for at least
185 48 hours, and 3) that pass through north India (50°–77°E, 22°–42.5°N). The northern limit of this
186 box, 42.5ºN, is more poleward than has been used previous studies (36.5ºN). This allows us to
187 better capture WD impacts over the Karakoram.

188

189 ## 2.2 Methods

190 **2.2.1) Lanczos filter**

191 To isolate the decadal signals, we linearly detrended all meteorological variables and the PDO index
192 for DJF. These datasets were then filtered using a 9-year running mean Lanczos filter, which is a
193 low-pass filter based on the sinc convolution (Duchon et al., 1979). The positive (negative) phase of
194 PDO is defined as years when the filtered DJF PDO index is greater than (less than) zero. We define
195 the negative epoch (PDO-) as two negative phases of PDO that occurred from 1948 to 1977 and
196 1989 to 2014, and the positive epoch (PDO+) as a positive phase of PDO that occurred from 1978

to 1988 (Fig.1b). Also, the detrended variables are used to conduct correlation and composite analyses. The Student's and Welch’s t-test are used in the study to determine the statistical significance of correlation and composite analyses, respectively.

2.2.2) Wavelet analysis

The PyCWT library (https://pycwt.readthedocs.io/en/latest/tutorial/cwt/) is used to calculate the cross-wavelet power spectrum. This library is based on the implementation by Torrence and Compo (1998). We employed the cross wavelet transform to calculate the wavelet spectrum between monthly time series of the PDO index and the area averaged monthly ERA5 snowfall over the KH region. The cross wavelet transform finds regions in time frequency space where the time series show high common power.

3) Results:

3.1) PDO and KH winter snowfall

This study aims to examine the long-term variability in DJF snowfall in the KH region in relation with the PDO from 1940 to 2022. There is a significant negative correlation between the lowpass-filtered and detrended time series of DJF PDO and DJF snowfall in the KH (Fig 1b), with a coefficient of -0.51. However, the PDO is not a single phenomenon, but rather a set of processes that occur in both the tropics and the extratropics and reflects the influence of various processes occurring at distinct timescales (Newman et al., 2016). More precisely, elevated sea surface temperature (SST) in the eastern tropical Pacific is linked to lower SST in the central and western North Pacific, while higher SST is observed in the eastern North Pacific (Deser et al. 2004; Newman et al., 2016). Thus, decadal variability in the North Pacific SSTs is linked to tropical Pacific decadal variability, specifically in terms of the long-lasting seasonal ENSO patterns (Newman et al., 2011; Wittenberg et al. 2014) as well as the ENSO like multidecadal oscillation (i.e., IPO; Zhang et al., 1997). Occasionally, the AMO may also influence multidecadal variability of the PDO (Zhang and Delworth, 2007). After excluding of the influences of ENSO and IPO, the correlation slightly increases to -0.53 and -0.54, and rises to -0.67 upon the elimination of the AMO's impact.

The spatial structure of the correlation between PDO and KH snowfall in winter (Fig. 2a) is significantly negative along the western and central Himalayas and much of the southern Karakoram, but positive over the Tibetan Plateau and north India. The snowfall in the KH region during the boreal autumn (SON) and spring (MAM) has a strong positive correlation with the PDO (not shown), whereas the summer monsoon season (JJA) displays a weak but positive correlation with the PDO. The different signs of the correlation suggest that the dynamic processes driving KH snowfall either vary by season, or the seasonal influence of the PDO on KH snowfall changes.

Figure 2b displays the regional distribution of the difference in detrended DJF snowfall between the negative and positive phases of PDO, hereafter referred to as PDO- and PDO+, respectively. The difference is significantly positive in the KH area, particularly over the southern part of the Karakoram region. DJF snowfall in the KH accounts for around 80-90% of total annual snowfall during the time period (not shown). During PDO+, DJF snowfall over KH is nearly 7% lower than the average seasonal snowfall, while during PDO- it is about 6% higher. It indicates that the difference in DJF snowfall in KH varies significantly depending on the phase of the PDO across several decades.

This strong relationship between PDO and snowfall in the KH is also demonstrated through a cross-wavelet frequency spectrum analysis between the unfiltered monthly time series of PDO index and snowfall over the KH from 1940 to 2022 (Fig. 2c). The band of strong and significant power in the period of ~1 year in the cross-wavelet indicates that the PDO and KH snowfall both have strong interannual variability. The well-known influence of ENSO on snowfall in the region (operating on interannual timescales) during DJF is also slightly modulated by the low-frequency oscillation of PDO. Another band of significant power exists in the 6-15 year range, indicating a high decadal scale correlation between these two time series. The significant power in the 6-15-year range occurred between 1940 and 1970 and again from 1998 to 2015, coinciding with the negative phases of the PDO. An insignificant weak power appeared within the same range from 1971 to 1988, coinciding with the positive phase of the PDO. A long band of strong power exists throughout the 16–20-year range, observed from 1950 to 1990, while a weaker power is shown from 2000 to 2022. This indicates that the low-frequency variability of KH snowfall is influenced by decadal oscillations over various time scales, while the interdecadal variability of KH snowfall is found to influenced by the phase of the PDO.

3.2) Sea Surface temperature (SST) variability during DJF

Figure 3a illustrates the well-known positive (or warm) phase of the PDO over the North Pacific, shown as a correlation between lowpass filtered and detrended sea surface temperature (SST) and PDO index during DJF. The correlation pattern also reveals a strong El-Nino like pattern in the eastern equatorial-tropical Pacific Ocean. For comparison, the correlation pattern between the DJF SST anomalies and the DJF snowfall anomalies in the KH region is shown in Figure 3b. This correlation strongly resembles the negative (or cool) phase of the PDO over the North Pacific Ocean. It is characterised by positive SST anomalies in the northwest Pacific and negative SST anomalies in the northeast Pacific. Additionally, there are negative SST correlations in the tropical eastern Pacific region and eastern Indian Ocean adjacent to Western Australia, while positive correlations are observed in the southwest Indian Ocean and across the northwest Atlantic Ocean. The correlation pattern in the southern Indian Ocean reveals the subtropical Indian Ocean Dipole signature (positive phase) (Behera & Yamagata, 2001; Yamagami & Tozuka, 2014).

3.3) Upper atmosphere circulation response with PDO and snowfall

To understand the anomalous atmospheric circulations that connect the PDO with anomalous DJF snowfall in the KH region, we computed the correlation of 200 hPa geopotential height with both the DJF PDO index (Fig. 4a) and DJF snowfall (Fig. 4b). The correlation pattern between the PDO and upper-level geopotential height shows a prominent upper-level trough over east China, Japan and the northwest Pacific, which is known as East Asian trough (EAT; Qin et al., 2018; Yin and Zhang, 2021). In contrast, the correlation pattern over the Caspian Sea, KH, and Lake Baikal region is associated with positive geopotential height anomalies. The EAT is a well-known upper atmospheric response to the positive phase of PDO to the East Asia-North Pacific region during the Northern Hemisphere winter (Newman et al, 2016; Qin et al., 2018; Yin and Zhang, 2021). The intensity of the EAT is strongly linked to the strength of the winter monsoon in East Asia and the tilt in the EAT axis is connected to midlatitude baroclinic processes, such as the eddy-driven jet or WD tracks over the East Asia-North Pacific region (Wang et al., 2009). Therefore, changes in location and intensity of the EAT can lead to, or otherwise indicate, regional climate anomalies, such as temperature in the upper troposphere which subsequently influence DJF precipitation in East Asia as well as the KH during the positive phase of the PDO.

These patterns change sign during negative phases of PDO, when KH snowfall is enhanced, implying an anomalous upper-level trough to the west of the Karakoram, consistent with increased WD frequency or intensity. The correlation between upper-level geopotential height and snowfall has a similar pattern to the PDO-geopotential correlation, but as expected, with reversed sign. The correlation pattern exhibits a strong ridge (or a weakened EAT) over the northwest Pacific and Japan characterised by the significant positive geopotential height anomalies. The negative correlation to the west of the KH area shows a trough, which is stronger than the positive correlation between PDO and geopotential height, indicating the linkage of seasonal snowfall to the passage of WDs is stronger than the link between the PDO and WDs. Both, however, are important. The appearance of the anomalous trough in both pairs of correlations implies that the PDO may affect KH snowfall by somehow modulating WD activity. Therefore, it is essential to understand how decadal fluctuations in DJF snowfall in the KH are driven by WDs and how the PDO influences WD behaviour. This can be accomplished by investigating the DJF STJ, followed by a detailed investigation of the WDs.

3.4) Modulation of WD and Subtropical Westerly Jet by the PDO

To further illustrate the above relationship between PDO and DJF snowfall in KH, we examine the composite differences in 200 hPa wind, geopotential height, and temperature (Fig. 5) between PDO- and PDO+. Figure 5a displays the difference in 200 hPa circulation over East Asia, Arabian Peninsula and northwest Pacific region. During the PDO-, there is a large negative geopotential height anomaly to the north of KH region, which extends from the Caspian Sea-Arabian Peninsula to KH. Strong westerlies are observed to the south of this trough with a stronger STJ prevailing across KH during the PDO-. An anomalous trough in the upper atmosphere is indicative of increased WD frequency (or intensity) and the frequency of WDs is strongly affected by variations in both the latitude and intensity of the STJ (Dimri et al., 2015; Hunt et al., 2017, 2018) over South Asia. Therefore, we now focus on understanding the relationship between the PDO and the STJ.

Upper-level jets are thermal wind responses to upper-level meridional temperature gradients. In Fig 5b, we show the difference in mid-to-upper (from 500 hPa to 300 hPa) tropospheric temperature between PDO- and PDO+. A quadrupole in the upper air temperature gradient is present across the KH, Tibetan Plateau (TP) and the northwest Pacific region during PDO-. Over the Pacific, this is effectively a direct response to the anomalous surface heating provided by the PDO. Anomalous

warm SSTs over the northwest Pacific lead to adiabatic cooling near the tropopause, which results in deep convection over the Maritime Continent during the PDO- (e.g., Wang et al., 2016). Upstream, over continental Asia, the relationship is more complicated and is probably a wave response to the direct forcing over the ocean. Therefore, a strongly enhanced meridional temperature gradient over the KH and TP, leading to a stronger and more meridionally-locked STJ.

Figure 5c displays the lowpass filtered time series of latitude and strength of the DJF STJ. During the PDO-, the STJ tends to sit slightly further north but is also substantially stronger. The correlation of the time series of the strength of DJF STJ with DJF PDO is significantly negative (-0.22), and the correlation between DJF STJ strength and DJF snowfall in KH is strong positive (0.51). The positive (negative) phase of the PDO enhances the movement of the STJ towards the south (north) through a response to the decreased (increased) SST over the northwest Pacific and modulates the cyclonic (anticyclonic) circulation over the northwest Pacific and adjacent maritime continents (Matsumura & Horinouchi, 2016). During PDO-, we observed a quadrupole in the anomalous upper-level temperature gradient (Fig. 5b), resulting in a negative anomaly in the temperature gradient and an anticyclonic circulation (Fig. 5a) over the TP. Thus, by modulating the STJ, the negative phase of the PDO leads to more frequent (more intense) WDs at slightly higher latitudes than usual (e.g. into the Karakoram, where the signal is the strongest).

The presence of a stronger STJ along with a wave-like pattern of trough (anomalous cyclone) over the northern region of KH, and a ridge (anomalous TP anticyclone) in the upper atmosphere, increases the occurrence of WDs over KH during the PDO-. After examining the impact of the PDO on the STJ, we now quantify its influence on WDs directly. Maps of the difference in the frequency of DJF WDs between PDO- and PDO+ (Fig. 6a) indicate that WDs are more frequent (with a 9% higher frequency) over the KH region during PDO- compared to PDO+. Also, the frequency of WDs is found to be reduced by around 3% in both the northern and southern regions of the KH during PDO- compared to PDO+. These WDs are observed to be more intense in the vicinity of the Caspian Sea and north of the KH during PDO- rather than PDO+ (not shown).

3.5) Atmospheric-ocean response of PDO on moisture transport in KH

Increased frequency and intensity of WDs have a significant impact on precipitation in the KH and surrounding region because they govern southwesterly moisture transport from the Arabian Sea (Baudouin et al., 2021; Hunt and Dimri 2021). The composite difference of DJF VIMF and VIMFC between PDO- and PDO+ is now examined to determine the response of moisture transport to the PDO and its subsequent effect on the KH (Fig. 6b). The average difference of VIMFC between PDO- and PDO+ is about 0.8×10^{-5} kg m^{-2} s^{-1} within KH region. An advection of moisture from the Black Sea, Red Sea, and eastern Mediterranean Sea through the Arabian Peninsula/Arabian Sea towards the KH in westerly fashion is observed. The precipitation associated with WDs is mostly determined by their intensity and proximity to the Arabian Sea (Baudouin et al., 2020). The variations in the moisture transport across the Arabian Peninsula/Arabian Sea are not directly linked to changes in VIMF over the northwest Pacific, but the presence of more WDs south of the strong DJF STJ over KH clearly result in greater moisture transport towards KH during PDO-. Hence, the anomalous moisture transport nearly perpendicular to KH, results in increased moisture flux convergence about 16% greater during the PDO- compared to the PDO+ and leads to greater precipitation in the region during PDO-.

4) Conclusion and Discussion:

The recent impacts of climate change over the KH, particularly in mean and extreme winter precipitation, have been largely attributed largely to anthropogenic forcing, such as greenhouse gases, aerosols, and changes in land use. However, these changes cannot be solely explained by natural forcing (Krishnan et al., 2018). Oceanic conditions, especially changes in SSTs over the equatorial-tropical Pacific and north Pacific, play an important role in driving interdecadal variability in atmospheric circulation and hence winter precipitation over the KH.

DJF snowfall in the KH accounts for around 80-90% of total annual snowfall during the time period, hence a 15% difference in DJF snowfall can have a significant influence on agriculture in this region, especially since most of the rivers in this region, such as tributaries of Indus, Tarim and Ganges are partially fed by snowmelt in the spring and later seasons (Armstrong et al., 2018). Understanding the interdecadal variability and its relationship with the PDO is important for understanding the long-term climate of the KH. We have analysed the long-term variability in winter snowfall over the KH due to PDO by using ERA5 reanalysis data from 1940 to 2022.We found that a strong negative correlation of -0.51 between the PDO and DJF snowfall in the KH.

Mean KH snowfall during DJF is approximately 6% greater than the DJF seasonal average during PDO-, and 7% lower during PDO+.

PDO associated anomalous warming of SST in the northwest Pacific modulates the snowfall in the KH via changes in upper-level temperatures over the Pacific and Asia. The warm SSTs lead to increased deep convection and subsequent upper-tropospheric adiabatic cooling over the Pacific. During PDO-, the anomalous heating of the tropospheric column over North Pacific leads to a wave like pattern with an upper-level trough over the north of KH and upper-level ridge over the Tibetan Plateau. This results in a stronger STJ to the west of, and over, the KH, before it is deflected northwards over the Tibetan Plateau. There is a strong positive correlation between the strength of DJF STJ and DJF snowfall in KH, with a correlation coefficient of 0.51, and a significant negative correlation between the strength of STJ and PDO, with a correlation coefficient of -0.22 during DJF at decadal scale. These results indicate a wave response over KH to the direct forcing of the north Pacific Ocean.

These anomalous jet conditions over KH are linked to a higher occurrence of WDs across the region. Using a track catalogue, we found that WDs are 9% more frequent across the KH and drop by approximately 3% in both the northern and southern regions of the KH during PDO- compared to PDO+. However, the WDs are found to be more intense in the vicinity of the Caspian Sea and north of the KH during PDO- rather than PDO+, which is not shown in this study. This increase in WD frequency results in anomalous moisture transport from the Arabian Sea, Black Sea, Red Sea, and eastern Mediterranean Sea towards the KH. The moisture transport is almost perpendicular to the orography of the KH, leading to a strong moisture convergence about 16% greater during the PDO- compared to the PDO+ and thus increased DJF precipitation in the region during the negative phases of the PDO.

Our findings highlight the importance of considering interdecadal variability when trying to quantify the effects of anthropogenic climate change in the KH. The recent PDO- has led to increased WD activity, and hence increased winter snowfall over this region, and may be masking the effects of climate change. More research is needed to disentangle climate change from the effects of interdecadal variability over this vulnerable region, so that policymakers can be better informed. The uncertainty in the snowfall and precipitation datasets, along with the limitations of the short timeseries available from reanalysis for examining decadal oscillations, are insufficient to demonstrate such studies. Future long-term climate simulations could be used for subsequent work

if the models accurately represent the interaction between the PDO and snowfall/precipitation in this region.

5) List of figures:

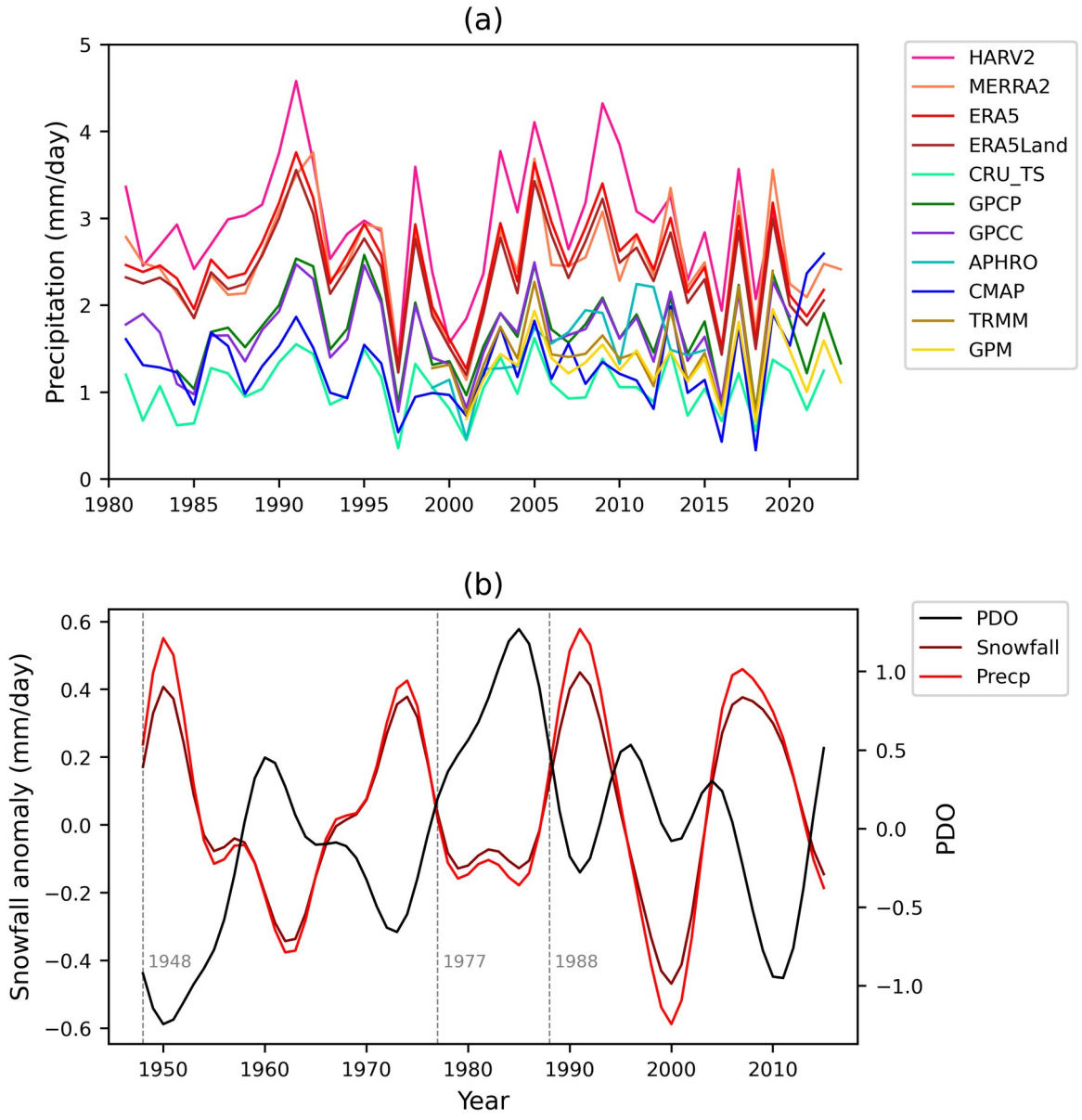

Figure 1: (a) Seasonal variability of DJF precipitation in the KH region (highlighted by a green box in Fig. 2a&b; 73º – 78º E, 33º – 38º N) from ERA5, ERA5-land, MERRA2, HARv2, CRU_TS, GPCP, GPCC, and CMAP during the period from 1980 to 2020, APHRODITE from 1998 to 2015, TRMM from 1998 to 2019, and GPM from 2000 to 2023. (b) Time series of 9-year filtered DJF PDO index and area-averaged DJF ERA5 snowfall (and precipitation)

anomalies over the KH region from 1940 to 2022. The vertical grey lines represent phase transitions of PDO.

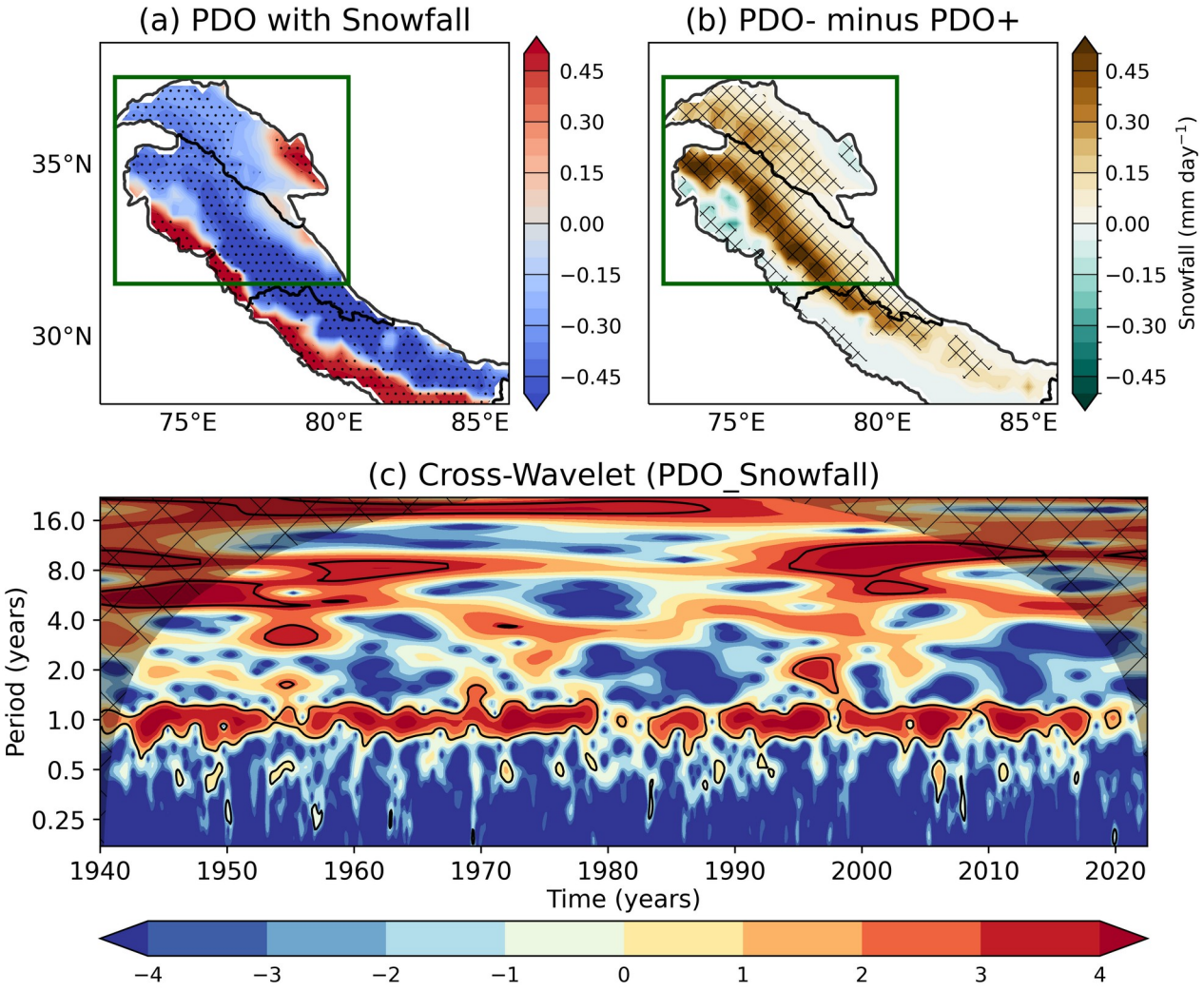

Figure 2: (a) Spatial map of correlation between the 9-year filtered PDO index and the snowfall (mm) over the KH region (cropped by the shapefile of the traditional boundaries of the Karakoram-Western and Central Himalaya; highlighted by a green box; 73° – 78° E, 33° – 38° N) during DJF, and (b) composite difference of DJF snowfall (mm) between negative and positive epoch of PDO, (c) cross-wavelet of DJF snowfall (mm) over the KH and DJF PDO index from 1940 to 2022. Traditional boundaries of Karakoram-Western and Central Himalayan regions are marked by thick black lines in (a) and (b). Stippling in (a) and (b) denotes regions where the correlation and composite differences are significant at a 95% confidence level, as determined by the two-tailed Student's t-test and Welch's t-test,

respectively. Black line contours on the power spectra in (c) indicate where the spectral power of the cross-wavelet is significantly greater than zero at a 95% confidence level.

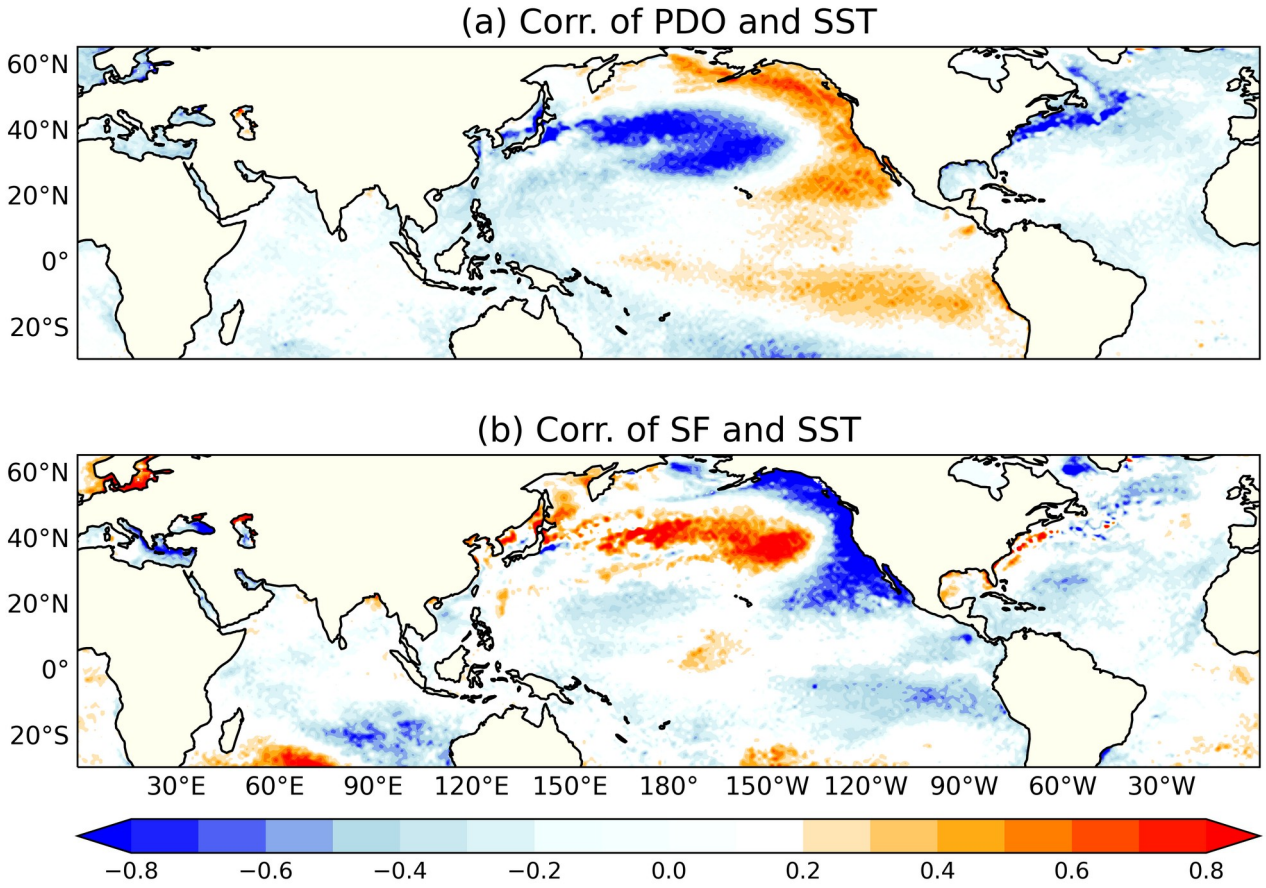

Figure 3: Spatial map of correlation of the 9-year filtered (a) DJF PDO index, and (b) area averaged DJF snowfall over the KH region (as defined in Fig.2) with 9-year filtered DJF sea surface temperature from 1940 to 2022. The correlations patterns are statistically significant at the 95% confidence level, as determined by the two tailed student's t-test.

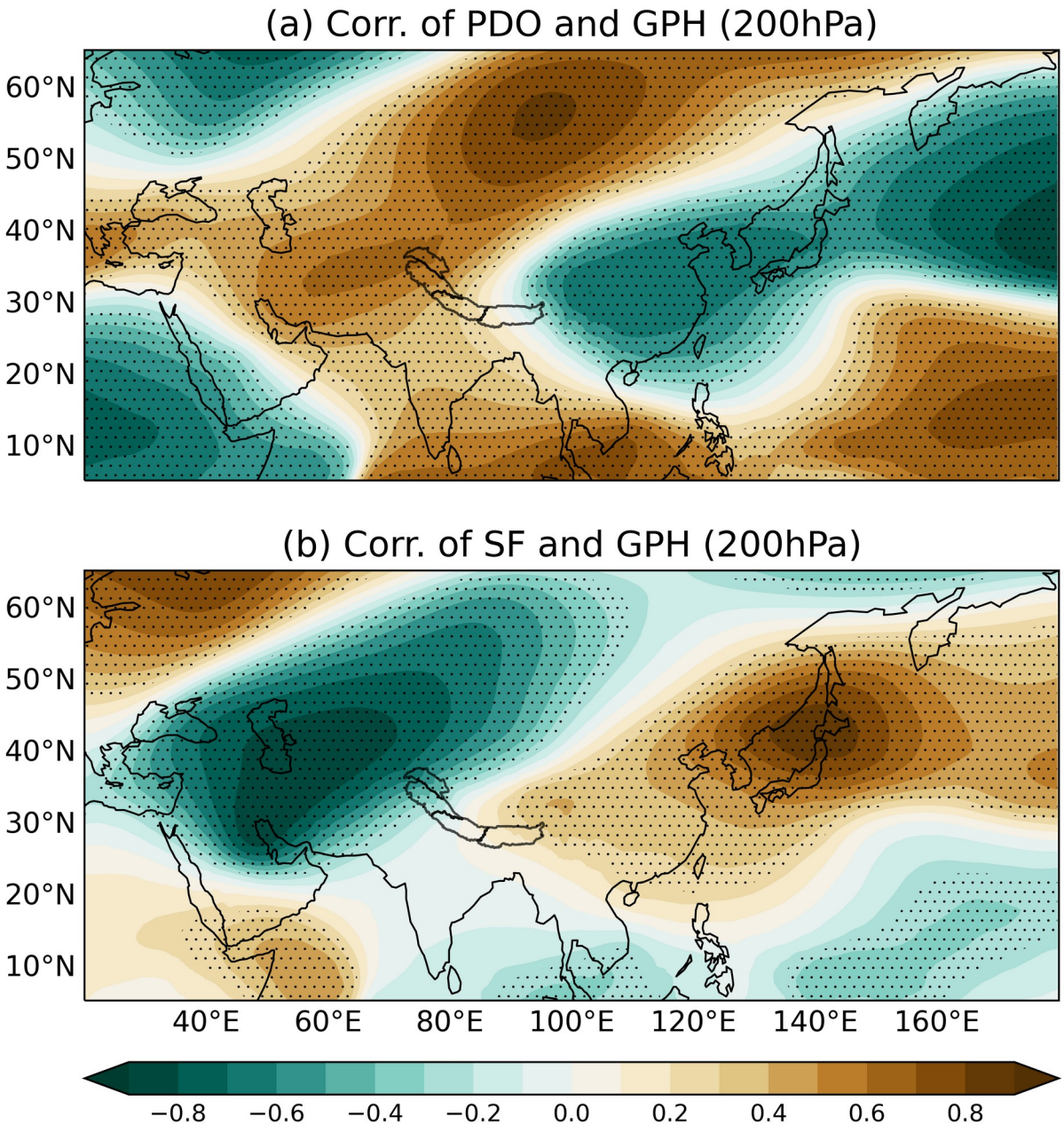

476 **Figure 4: Spatial map of correlation of the 9-year filtered (a) DJF PDO index, and (b) area**
477 **averaged DJF snowfall (mm) over the KH region (as defined in Fig.2) with 9-year filtered DJF**
478 **geopotential height at 200hPa (m) from 1940 to 2022. Stippling in (a) and (b) indicate where**
479 **the correlations are significant at a 95% confidence level, as determined by the two tailed**
480 **student's t-test.**

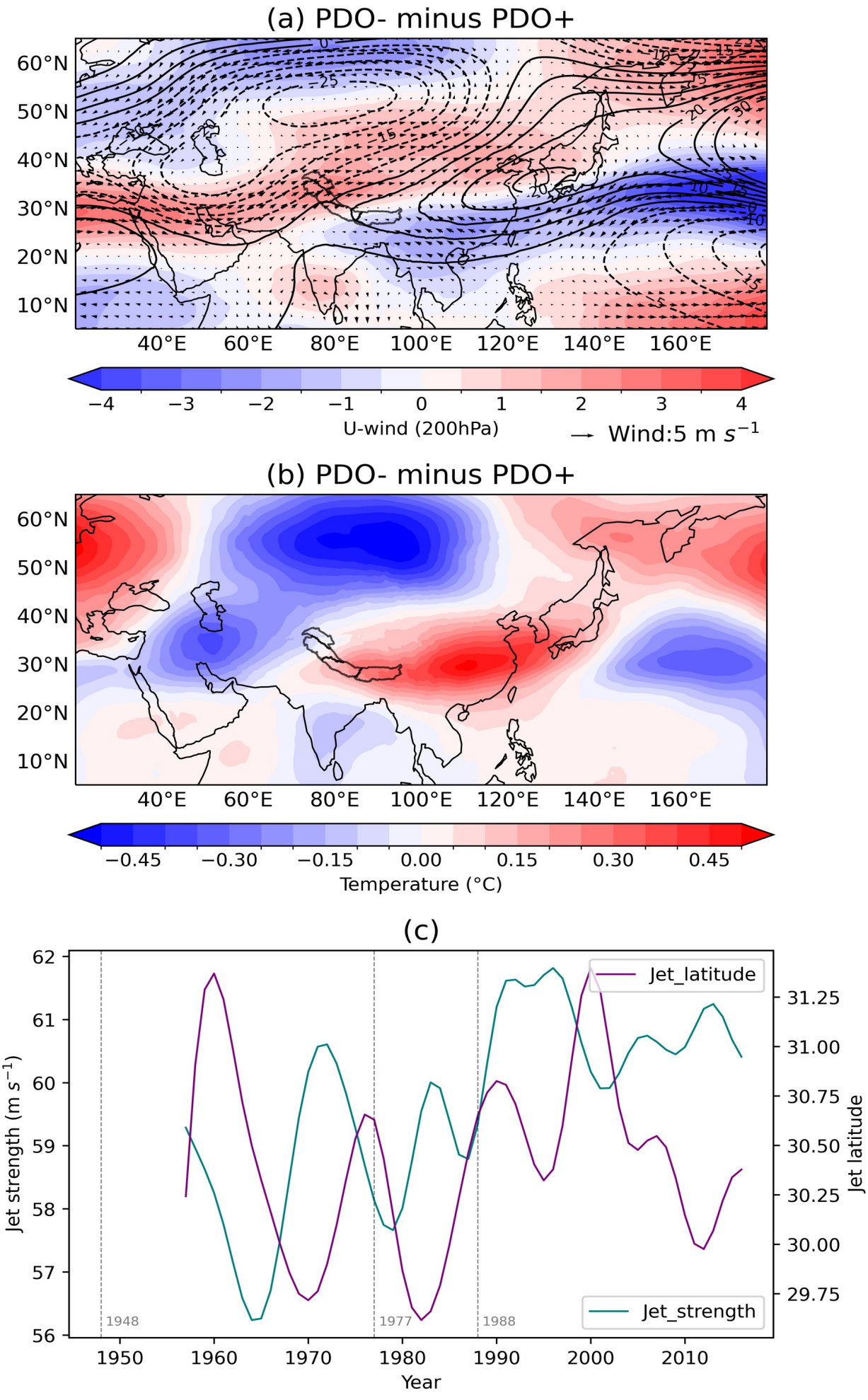
(a) PDO- minus PDO+
60°N
50°N
40°N
30°N
20°N
10°N
40°E
60°E
80°E
100°E
120°E
140°E
160°E
−4
−3
−2
−1
0
1
2
3
4
U-wind (200hPa)
Wind:5 m s^{-1}
(b) PDO- minus PDO+
−0.45
−0.30
−0.15
0.00
0.15
0.30
0.45
Temperature (°C)
(c)
Jet_latitude
Jet_strength
Jet strength (m s^{-1})
Jet latitude
Year
1948
1977
1988
62
61
60
59
58
57
56
31.25
31.00
30.75
30.50
30.25
30.00
29.75
1950
1960
1970
1980
1990
2000
2010

Figure 5: Composite difference of (a) U-wind (colours; m s^{-1}), wind (vectors; m s^{-1}), and geopotential height (contours; m), (b) vertically averaged temperature (ºC) from 300hPa to 500hPa level during DJF between negative and positive epoch of PDO, (c) time series of 9-year filtered strength (magenta; m s^{-1}), and latitude (blue) of DJF subtropical westerly jet over the KH region from 1940 to 2022.

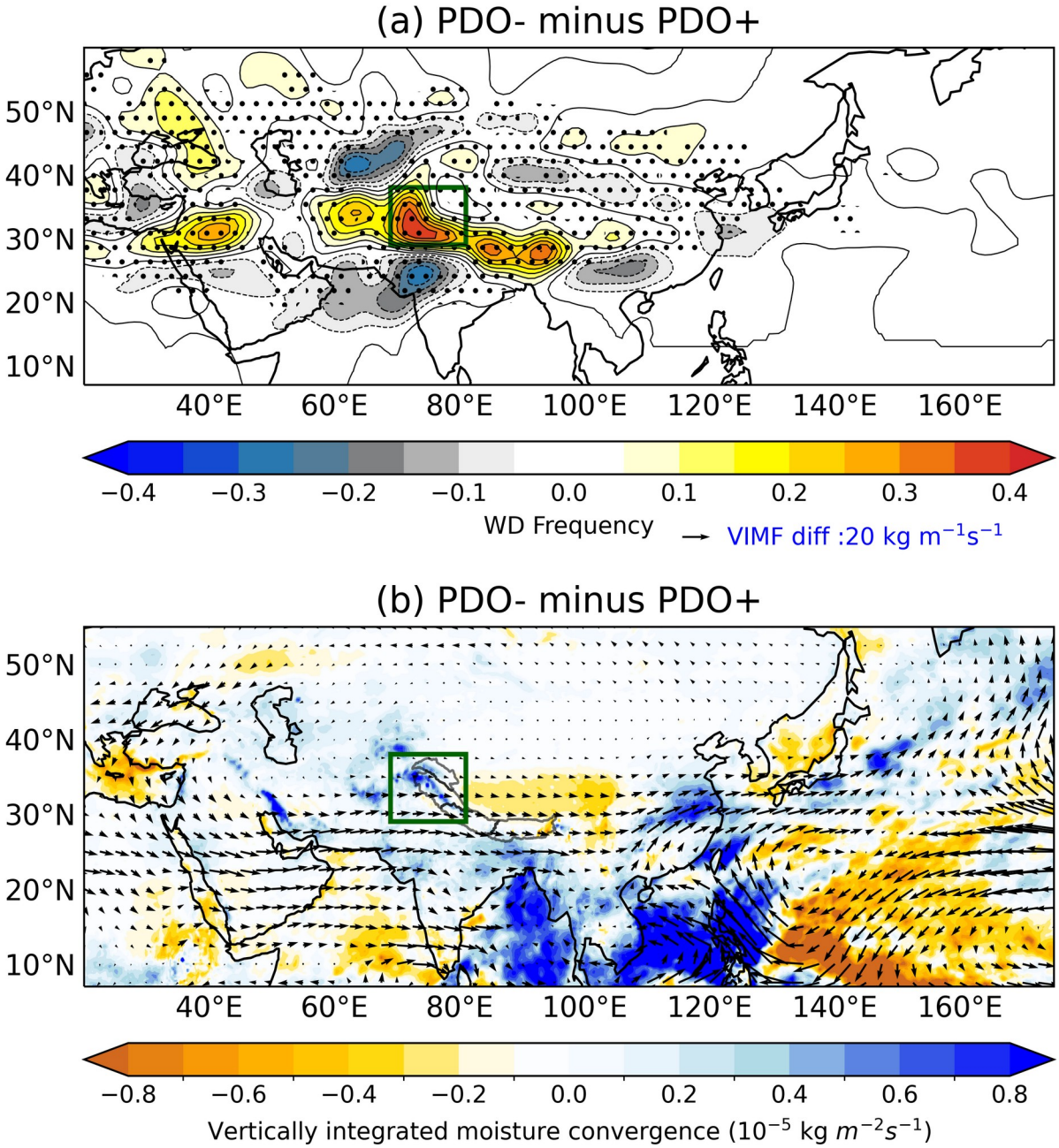

Figure 6: Composite difference of (a) WD frequency, and (b) vertically integrated moisture flux (vectors; kg m^{-1} s^{-1}) and vertically integrated moisture convergence (colours; kg m^{-2} s^{-1}) during DJF between negative and positive epoch of PDO from 1940 to 2022. Stippling in (a)

indicates where the differences are significant at a 95% confidence level, as determined by the two tailed Welch's t-test. Green box in (a) and (b) highlights the KH region (as defined in Fig.2).

Author Contributions:

Priya Bharati: conceptualization; formal analysis; methodology; investigation; software; visualization; writing original draft. **Kieran M. R. Hunt:** conceptualization; methodology; software; writing - review and editing. **Pranab Deb:** supervision; conceptualization; writing – review and editing.

Competing interests:

The contact author has declared that none of the authors has any competing interests.

Acknowledgements:

The work is carried at CORAL, Indian Institute of Technology Kharagpur under supervision of Pranab Deb. Priya Bharati is funded through the Ministry of Science and Technology, Government of India, Council of Scientific and Industrial Research (CSIR; 09/081(1371)/2019-EMR-I). KMRH is supported by a NERC Independent Research Fellowship (MITRE; NE/W007924/1).

References:

Adler, R., Sapiano, M., Huffman, G., Bolvin, D., Gu, G., Wang, J., and Becker, A.: The new version 2.3 of the Global Precipitation Climatology Project (GPCP) monthly analysis product, University of Maryland, April, 1072-1084, 2016.

Aggarwal, D., Chakraborty R., and Attada, R.: Investigating bi-decadal precipitation changes over the Northwest Himalayas during the pre-monsoon: role of Pacific decadal oscillations, Climate Dynamics, 62(2), 1203-1218, 2024. https://doi.org/10.1007/s00382-023-06969-3

Archer, D. R., and Fowler, H. J.: Spatial and temporal variations in precipitation in the Upper Indus Basin, global teleconnections and hydrological implications, Hydrology and Earth System Sciences, 8(1), 47-61, 2004. https://doi.org/10.5194/hess-8-47-2004

Armstrong, R. L., Rittger, K., Brodzik, M. J., Racoviteanu, A., Barrett, A. P., Khalsa, S. J. S., and Armstrong, B.: Runoff from glacier ice and seasonal snow in High Asia: separating melt water sources in river flow, Regional Environmental Change, 19, 1249-1261, 2019. https://doi.org/10.1007/s10113-018-1429-0

Barlow, M., Wheeler, M., Lyon, B., and Cullen, H.: Modulation of daily precipitation over southwest Asia by the Madden–Julian oscillation, Monthly weather review, 133(12), 3579-3594, 2005. https://doi.org/10.1175/MWR3026.1

Basu, S., Bieniek, P. A., and Deoras, A.: An investigation of reduced western disturbance activity over Northwest India in November-December 2015 compared to 2014-A case study, Asia-Pacific Journal of Atmospheric Sciences,53, 75-83, 2017. DOI:10.1007/s13143-017-0006-7

Baudouin, J. P., Herzog, M., and Petrie, C. A.: Cross-validating precipitation datasets in the Indus River basin, Hydrology and Earth System Sciences, 24(1), 427-450, 2020. https://doi.org/10.5194/hess-24-427-2020

Beck, H., Pan, M., Roy, T., and Wood, E. F.: Evaluation of 27 precipitation datasets using Stage-IV gauge-radar data for the CONUS, AGU Fall Meeting 2018, 2018.

Behera, S. K., and Yamagata, T.: Subtropical SST dipole events in the southern Indian Ocean, Geophysical Research Letters, 28(2), 327-330, 2001. https://doi.org/10.1029/2000GL011451

Bharati, P., Deb, P., Hunt, K., Orr, A., and Dash, M. K.: ENSO-induced latitudinal variation of the subtropical jet modulates extreme winter precipitation over the Western Himalaya, Advances in Atmospheric Sciences. doi: 10.1007/s00376-024-4057-2

Bolch, T., Kulkarni, A., Kääb, A., Huggel, C., Paul, F., Cogley, J. G., and Stoffel, M.: The state and fate of Himalayan glaciers, Science, 336(6079), 310-314, 2012. DOI: 10.1126/science.1215828

Bonekamp, P. N., De Kok, R. J., Collier, E., and Immerzeel, W. W.: Contrasting meteorological drivers of the glacier mass balance between the Karakoram and central Himalaya, Frontiers in Earth Science, 7, 107, 2019. https://doi.org/10.3389/feart.2019.00107

Bookhagen, B., and Burbank, D. W.: Toward a complete Himalayan hydrological budget: Spatiotemporal distribution of snowmelt and rainfall and their impact on river discharge, Journal of Geophysical Research: Earth Surface, 115(F3), 2010. https://doi.org/10.1029/2009JF001426

Bosilovich, M. G., Chen, J., Robertson, F. R., and Adler, R. F.: Evaluation of global precipitation in reanalyses, Journal of applied meteorology and climatology, 47(9), 2279-2299, 2008. https://doi.org/10.1175/2008JAMC1921.1

Cannon, F., Carvalho, L. M., Jones, C., and Bookhagen, B.: Multi-annual variations in winter westerly disturbance activity affecting the Himalaya, Climate dynamics, 44, 441-455, 2015. DOI 10.1007/s00382-014-2248-8

Cannon, F., Carvalho, L. M., Jones, C., Hoell, A., Norris, J., Kiladis, G. N., and Tahir, A. A.: The influence of tropical forcing on extreme winter precipitation in the western Himalaya, Climate Dynamics, 48, 1213-1232, 2017. DOI 10.1007/s00382-016-3137-0

598 Dahri, Z. H., Moors, E., Ludwig, F., Ahmad, S., Khan, A., Ali, I., and Kabat, P.: Adjustment of
599 measurement errors to reconcile precipitation distribution in the high-altitude Indus basin,
600 International Journal of Climatology 2018; 38: 3842–3860, 2018. DOI: 10.1002/joc.5539

601

602 Dai, A. (2013). The influence of the inter-decadal Pacific oscillation on US precipitation during
603 1923–2010, Climate dynamics, 41(3), 633-646, 2013. DOI 10.1007/s00382-012-1446-5

604

605 de Kok, R. J., Tuinenburg, O. A., Bonekamp, P. N., and Immerzeel, W. W.: Irrigation as a potential
606 driver for anomalous glacier behavior in High Mountain Asia, Geophysical research letters, 45(4),
607 2047-2054, 2018. https://doi.org/10.1002/2017GL076158

608

609 Deser, C., Phillips, A. S., & Hurrell, J. W.: Pacific interdecadal climate variability: Linkages
610 between the tropics and the North Pacific during boreal winter since 1900, Journal of Climate,
611 17(16), 3109-3124, 2004. https://doi.org/10.1175/1520-0442(2004)017<3109:PICVLB>2.0.CO;2

612

613 Dimri, A. P., Niyogi, D., Barros, A. P., Ridley, J., Mohanty, U. C., Yasunari, T., and Sikka, D. R.:
614 Western disturbances: a review, Reviews of Geophysics, 53(2), 225-246, 2015.
615 https://doi.org/10.1002/2014RG000460

616

617 Dimri, A. P., and Dash, S. K.: Wintertime climatic trends in the western Himalayas, Climatic
618 Change, 111, 775-800, 2012. DOI 10.1007/s10584-011-0201-y

619

620 Dimri, A. P., and Niyogi, D.: Regional climate model application at subgrid scale on Indian winter
621 monsoon over the western Himalayas, International Journal of Climatology, 33(9), 2013.

622

623 Dimri, A. P.: Relationship between ENSO phases with Northwest India winter precipitation,
624 International Journal of Climatology, 33(8), 1917-1923, 2013. DOI: 10.1002/joc.3559

625

626 Dollan, I. J., Maina, F. Z., Kumar, S. V., Nikolopoulos, E. I., and Maggioni, V.: An assessment of
627 gridded precipitation products over High Mountain Asia, Journal of Hydrology: Regional Studies,
628 52, 101675, 2024. https://doi.org/10.1016/j.ejrh.2024.101675

629

630 Dong, B., and Dai, A.: The influence of the interdecadal Pacific oscillation on temperature and
631 precipitation over the globe, Clim Dyn, 45, 2667-2681, 2015. DOI 10.1007/s00382-015-2500-x

632

633 Duchon, C. E.: Lanczos filtering in one and two dimensions, Journal of Applied Meteorology and
634 Climatology, 18(8), 1016-1022, 1979. https://doi.org/10.1175/1520-
635 0450(1979)018%3C1016:LFIOAT%3E2.0.CO;2

636

637 Enfield, D. B., Mestas-Nuñez, A. M., and Trimble, P. J.: The Atlantic multidecadal oscillation and
638 its relation to rainfall and river flows in the continental US, Geophysical research letters, 28(10),
639 2077-2080, 2001. https://doi.org/10.1029/2000GL012745

640

641 Farinotti, D., Immerzeel, W. W., de Kok, R. J., Quincey, D. J., and Dehecq, A.: Manifestations and
642 mechanisms of the Karakoram glacier Anomaly, Nature geoscience, 13(1), 8-16, 2020.
643 https://doi.org/10.1038/s41561-019-0513-5

644

645 Filippi, L., Palazzi, E., von Hardenberg, J., and Provenzale, A.: Multidecadal variations in the
646 relationship between the NAO and winter precipitation in the Hindu Kush–Karakoram, Journal of
647 climate, 27(20), 7890-7902, 2014. https://doi.org/10.1175/JCLI-D-14-00286.1

648

649 Forsythe, N., Fowler, H. J., Li, X. F., Blenkinsop, S., and Pritchard, D.: Karakoram temperature and
650 glacial melt driven by regional atmospheric circulation variability, Nature Climate Change, 7(9),
651 664-670, 2017. DOI: 10.1038/NCLIMATE3361

652

653 Fowler, H. J., and Archer, D. R.: Conflicting signals of climatic change in the Upper Indus Basin,
654 Journal of climate, 19(17), 4276-4293, 2006. https://doi.org/10.1175/JCLI3860.1

Gardelle, J., Berthier, E., & Arnaud, Y.: Slight mass gain of Karakoram glaciers in the early twenty-first century, Nature geoscience, 5(5), 322-325, 2012. DOI: 10.1038/NGEO1450

Gelaro, R., McCarty, W., Suárez, M. J., Todling, R., Molod, A., Takacs, L., and Zhao, B.: The modern-era retrospective analysis for research and applications, version 2 (MERRA-2), Journal of climate, 30(14), 5419-5454, 2017. https://doi.org/10.1175/JCLI-D-16-0758.1

Harris, I. P. D. J., Jones, P., Osborn, T., and Lister, D.: Updated high-resolution grids of monthly climatic observations-the CRU TS3. 10 Dataset, International journal of climatology, 34, 623-642, 2014.

Hersbach, H., de Rosnay, P., Bell, B., Schepers, D., Simmons, A., Soci, C., and Berrisford, P.: Operational global reanalysis: Progress, future directions and synergies with NWP (ERA report Series No. 27), European Centre for Medium Range Weather Forecasts: Reading, UK, 2018.

Hewitt, K.: The Karakoram anomaly? Glacier expansion and the 'elevation effect,' Karakoram Himalaya, Mountain Research and Development, 332-340, 2005. https://doi.org/10.1659/0276-4741(2005)025[0332:TKAGEA]2.0.CO;2

Hewitt, K. (2014).: Glaciers of the Karakoram Himalaya, Encyclopedia of Snow, Ice and Glaciers, edited by: Singh, VP, Singh, P., and Haritashya, UK, Springer Netherlands, Dordrecht, 429-436, 2014. DOI 10.1007/978-94-007-6311-1

Hoell, A., Barlow, M., and Saini, R.: Intraseasonal and seasonal-to-interannual Indian Ocean convection and hemispheric teleconnections, Journal of Climate, 26(22), 8850-8867, 2013. https://doi.org/10.1175/JCLI-D-12-00306.1

Huffman, G. J., Bolvin, D. T., Nelkin, E. J., Wolff, D. B., Adler, R. F., Gu, G., and Stocker, E. F.: The TRMM multisatellite precipitation analysis (TMPA): Quasi-global, multiyear, combined-sensor precipitation estimates at fine scales, Journal of hydrometeorology, 8(1), 38-55, 2007. https://doi.org/10.1175/JHM560.1

Huffman, G. J., Bolvin, D. T., Braithwaite, D., Hsu, K., Joyce, R., Xie, P., and Yoo, S. H.: NASA global precipitation measurement (GPM) integrated multi-satellite retrievals for GPM (IMERG), Algorithm theoretical basis document (ATBD) version, 4(26), 2020-05, 2015.

Hunt, K. M., Turner, A. G., and Shaffrey, L. C.: The evolution, seasonality and impacts of western disturbances, Q. J. R. Meteorol. Soc., 144(710), 278-290, 2018. DOI:10.1002/qj.3200

Hunt, K. M., and Fletcher, J. K.: The relationship between Indian monsoon rainfall and low-pressure systems, Climate Dynamics,53(3), 1859-1871, 2019. https://doi.org/10.1007/s00382-019-04744-x

Hu, X., and Yuan, W.: Evaluation of ERA5 precipitation over the eastern periphery of the Tibetan plateau from the perspective of regional rainfall events, International Journal of Climatology, 41(4), 2625-2637, 2021. DOI: 10.1002/joc.6980

Hunt, K. M., and Zaz, S. N.: Linking the North Atlantic Oscillation to winter precipitation over the Western Himalaya through disturbances of the subtropical jet, Climate Dynamics, 60(7), 2389-2403, 2023. https://doi.org/10.1007/s00382-022-06450-7

Hunt, K. M., Baudouin, J. P., Turner, A. G., Dimri, A. P., Jeelani, G., Pooja, and Palazzi, E.: Western disturbances and climate variability: a review of recent developments, EGUsphere,2024, 1-106, 2024. https://doi.org/10.5194/egusphere-2024-820

Javed, A., Kumar, P., Hodges, K. I., Sein, D. V., Dubey, A. K., and Tiwari, G.: Does the recent revival of western disturbances govern the Karakoram anomaly?, Journal of Climate, 35(13), 4383-4402, 2022. DOI: 10.1175/JCLI-D-21-0129.1

Joshi, M. K., Rai, A., and Pandey, A. C.: Validation of TMPA and GPCP 1DD against the ground truth rain-gauge data for Indian region, International journal of climatology,33(12), 2013. DOI: 10.1002/joc.3612

Kääb, A., Berthier, E., Nuth, C., Gardelle, J., and Arnaud, Y.: Contrasting patterns of early twenty-first-century glacier mass change in the Himalayas, Nature, 488(7412), 495-498, 2012. doi:10.1038/nature11324

Kamil, S., Almazroui, M., Kang, I. S., Hanif, M., Kucharski, F., Abid, M. A., and Saeed, F.: Long-term ENSO relationship to precipitation and storm frequency over western Himalaya–Karakoram–Hindukush region during the winter season, Climate Dynamics, 53, 5265-5278, 2019. https://doi.org/10.1007/s00382-019-04859-1

Kapnick, S. B., Delworth, T. L., Ashfaq, M., Malyshev, S., and Milly, P. C.: Snowfall less sensitive to warming in Karakoram than in Himalayas due to a unique seasonal cycle, Nature Geoscience, 7(11), 834-840, 2014. DOI: 10.1038/NGEO2269

Kar, S. C., and Rana, S.: Interannual variability of winter precipitation over northwest India and adjoining region: impact of global forcings, Theoretical and applied climatology, 116, 609-623, 2014. DOI 10.1007/s00704-013-0968-z

Kishore, P., Jyothi, S., Basha, G., Rao, S. V. B., Rajeevan, M., Velicogna, I., and Sutterley, T. C.: Precipitation climatology over India: validation with observations and reanalysis datasets and spatial trends, Clim Dyn, 46, 541-556, 2016. DOI 10.1007/s00382-015-2597-y

Krishnan, R., Sabin, T. P., Madhura, R. K., Vellore, R. K., Mujumdar, M., Sanjay, J., and Rajeevan, M.: Non-monsoonal precipitation response over the Western Himalayas to climate change, Climate Dynamics, 52, 4091-4109, 2019. https://doi.org/10.1007/s00382-018-4357-2

Krishnan, R., and Sugi, M.: Pacific decadal oscillation and variability of the Indian summer monsoon rainfall, Climate Dynamics, 21, 233-242, 2003. DOI 10.1007/s00382-003-0330-8

Krishnamurthy, L., and Krishnamurthy, V. J. C. D.: Influence of PDO on South Asian summer monsoon and monsoon–ENSO relation, Climate dynamics, 42, 2397-2410, 2014. DOI 10.1007/s00382-013-1856-z

Krishnamurthy, L., and Krishnamurthy, V.: Decadal scale oscillations and trend in the Indian monsoon rainfall, Clim Dyn, 43, 319-331, 2014. DOI 10.1007/s00382-013-1870-1

Lang, T. J., and Barros, A. P.: Winter storms in the central Himalayas, Journal of the Meteorological Society of Japan. Ser. II, 82(3), 829-844, 2004. https://doi.org/10.2151/jmsj.2004.829

Mantua, N. J., Hare, S. R., and Zhang, Y.: A Pacific interdecadal climate oscillation with impacts on salmon production, Oceanographic Literature Review, 1(45), 36, 1998.

Ménégoz, M., Gallée, H., and Jacobi, H. W.: Precipitation and snow cover in the Himalaya: from reanalysis to regional climate simulations, Hydrology and Earth System Sciences, 17(10), 3921-3936, 2013. https://doi.org/10.5194/hess-17-3921-2013

Midhuna, T. M., and Dimri, A. P.: Impact of arctic oscillation on Indian winter monsoon, Meteorology and Atmospheric Physics, 131, 1157-1167, 2019. https://doi.org/10.1007/s00703-018-0628-z

769 Midhuna, T. M., Kumar, P., and Dimri, A. P.: A new Western Disturbance Index for the Indian
770 winter monsoon, Journal of Earth System Science, 129, 1-14, 2020. https://doi.org/10.1007/s12040-
771 019-1324-1

772

773 Newman, M., Shin, S. I., and Alexander, M. A. Natural variation in ENSO flavors, Geophysical
774 Research Letters, 38(14), 2011. https://doi.org/10.1029/2011GL047658

775

776 Newman, M., Alexander, M. A., Ault, T. R., Cobb, K. M., Deser, C., Di Lorenzo, E., and Smith, C.
777 A.: The Pacific decadal oscillation, revisited, Journal of Climate, 29(12), 4399-4427, 2016. DOI:
778 10.1175/JCLI-D-15-0508.1

779

780 Nischal, Attada, R., and Hunt, K. M.: Evaluating winter precipitation over the western Himalayas in
781 a high-resolution Indian regional reanalysis using multisource climate datasets, Journal of Applied
782 Meteorology and Climatology, 61(11), 1613-1633, 2022. https://doi.org/10.1175/JAMC-D-21-
783 0172.1

784

785 Norris, J., Carvalho, L. M., Jones, C., and Cannon, F.: WRF simulations of two extreme snowfall
786 events associated with contrasting extratropical cyclones over the western and central Himalaya,
787 Journal of Geophysical Research: Atmospheres, 120(8), 3114-3138, 2015.
788 https://doi.org/10.1002/2014JD022592

789

790 Norris, J., Carvalho, L. M., Jones, C., Cannon, F., Bookhagen, B., Palazzi, E., and Tahir, A. A.: The
791 spatiotemporal variability of precipitation over the Himalaya: evaluation of one-year WRF model
792 simulation, Climate Dynamics, 49, 2179-2204, 2017. DOI 10.1007/s00382-016-3414-y

793

794 Norris, J., Carvalho, L. M., Jones, C., and Cannon, F.: Deciphering the contrasting climatic trends
795 between the central Himalaya and Karakoram with 36 years of WRF simulations, Climate
796 Dynamics, 52, 159-180, 2019. https://doi.org/10.1007/s00382-018-4133-3

797

798 Palazzi, E., Von Hardenberg, J., and Provenzale, A.: Precipitation in the Hindu-Kush Karakoram
799 Himalaya: observations and future scenarios, Journal of Geophysical Research: Atmospheres,
800 118(1), 85-100, 2013. https://doi.org/10.1029/2012JD018697

801

802 Power, S., Casey, T., Folland, C., Colman, A., and Mehta, V.: Inter-decadal modulation of the
803 impact of ENSO on Australia, Climate dynamics, 15, 319-324, 1999.

804

805 Pritchard, H. D.: Asia's shrinking glaciers protect large populations from drought stress, Nature,
806 569(7758), 649-654, 2019. https://doi.org/10.1038/s41586-019-1240-1

807

808 Qin, M., Li, D., Dai, A., Hua, W., and Ma, H.: The influence of the Pacific Decadal Oscillation on
809 North Central China precipitation during boreal autumn, International Journal of Climatology, 38,
810 e821-e831, 2018. DOI: 10.1002/joc.5410

811

812 Rana, S., McGregor, J., and Renwick, J.: Precipitation seasonality over the Indian subcontinent: An
813 evaluation of gauge, reanalyses, and satellite retrievals, Journal of Hydrometeorology, 16(2), 631-
814 651, 2015. https://doi.org/10.1175/JHM-D-14-0106.1

815

816 Rana, S., McGregor, J., and Renwick, J.: Dominant modes of winter precipitation variability over
817 Central Southwest Asia and inter-decadal change in the ENSO teleconnection, Climate dynamics,
818 53, 5689-5707, 2019. https://doi.org/10.1007/s00382-019-04889-9

819

820 Ridley, J., Wiltshire, A., and Mathison, C.: More frequent occurrence of westerly disturbances in
821 Karakoram up to 2100, Science of the Total Environment, 468, S31-S35, 2013.
822 http://dx.doi.org/10.1016/j.scitotenv.2013.03.074

823

824 Schneider, U., Becker, A., Finger, P., Meyer-Christoffer, A. and Ziese, M.: GPCC full data monthly
825 product version 2018 at 0.25: monthly land-surface precipitation from rain-gauges built on GTS-
826 based and historical data, Global Precipitation Climatology Centre, 2018.

827

828 Singh, T., Saha, U., Prasad, V. S., and Gupta, M. D.: Assessment of newly-developed high
829 resolution reanalyses (IMDAA, NGFS and ERA5) against rainfall observations for Indian region,
830 Atmospheric Research, 259, 105679, 2021. https://doi.org/10.1016/j.atmosres.2021.105679

831

832 Syed, F. S., Giorgi, F., Pal, J. S., and Keay, K.: Regional climate model simulation of winter climate
833 over Central-Southwest Asia, with emphasis on NAO and ENSO effects, International journal of
834 climatology, 30(2), 220-235, 2010. DOI: 10.1002/joc.1887

835

836 Tahir, A. A., Chevallier, P., Arnaud, Y., and Ahmad, B.: Snow cover dynamics and hydrological
837 regime of the Hunza River basin, Karakoram Range, Northern Pakistan, Hydrology and Earth
838 System Sciences, 15(7), 2275-2290, 2011. https://doi.org/10.5194/hess-15-2275-2011

839

840 Wang, L., Chen, W., Zhou, W., and Huang, R.: Interannual variations of East Asian trough axis at
841 500 hPa and its association with the East Asian winter monsoon pathway, Journal of Climate, 22(3),
842 600-614,2009. https://doi.org/10.1175/2008JCLI2295.1

843

844 Wang, S., Huang, J., He, Y., and Guan, Y.: Combined effects of the Pacific decadal oscillation and
845 El Nino-southern oscillation on global land dry–wet changes, Scientific reports, 4(1), 6651, 2014.
846 DOI: 10.1038/srep06651

847

848 Wang, W., Matthes, K., Omrani, N. E., and Latif, M.: Decadal variability of tropical tropopause
849 temperature and its relationship to the Pacific Decadal Oscillation, Scientific reports, 6(1), 29537,
850 2016. DOI: 10.1038/srep29537

851

852 Wang, X., Tolksdorf, V., Otto, M., and Scherer, D.: High Asia Refined Analysis Version 2 (HAR
853 v2): a New Atmospheric Data Set for the Third Pole Region, EGU General Assembly Conference
854 Abstracts (p. 8756), 2020. DOI: 10.5194/egusphere-egu2020-8756

855

Wester, Philippus, Mishra, Arabinda, Mukherji, Aditi, Shrestha, Arun Bhakta (Eds.),: The Hindu Kush Himalaya Assessment: Mountains, Climate Change, Sustainability and People, Springer, HIMAP, 2020.

Wittenberg, A. T., Rosati, A., Delworth, T. L., Vecchi, G. A., and Zeng, F.: ENSO modulation: Is it decadally predictable?, Journal of Climate, 27(7), 2667-2681, 2014. https://doi.org/10.1175/JCLI-D-13-00577.1

Wu, B., and Wang, J.: Winter Arctic oscillation, Siberian high and East Asian winter monsoon, Geophysical research letters, 29(19), 3-1, 2002. https://doi.org/10.1029/2002GL015373

Wu, X., and Mao, J.: Interdecadal modulation of ENSO-related spring rainfall over South China by the Pacific Decadal Oscillation, Climate dynamics, 47, 3203-3220, 2016. DOI 10.1007/s00382-016-3021-y

Xie, P., and Arkin, P. A.: Global precipitation: A 17-year monthly analysis based on gauge observations, satellite estimates, and numerical model outputs, Bulletin of the american meteorological society, 78(11), 2539-2558, 1997. https://doi.org/10.1175/1520-0477(1997)078%3C2539:GPAYMA%3E2.0.CO;2

Yadav, R. K., Rupa Kumar, K., and Rajeevan, M.: Increasing influence of ENSO and decreasing influence of AO/NAO in the recent decades over northwest India winter precipitation, Journal of Geophysical Research: Atmospheres, 114(D12), 2009. doi:10.1029/2008JD011318

Yadav, R. K., Yoo, J. H., Kucharski, F., and Abid, M. A.: Why is ENSO influencing northwest India winter precipitation in recent decades?, Journal of Climate, 23(8), 1979-1993, 2010. DOI: 10.1175/2009JCLI3202.1

884 Yadav, R. K., Rupa Kumar, K., and Rajeevan, M.: Role of Indian Ocean sea surface temperatures in
885 modulating northwest Indian winter precipitation variability, Theor. Appl. Climatol., 87, 73-83,
886 2007. DOI 10.1007/s00704-005-0221-5

887

888 Yamagami, Y., and Tozuka, T.: Interdecadal changes of the Indian Ocean subtropical dipole mode,
889 Clim Dyn, 44, 3057-3066, 2015. DOI 10.1007/s00382-014-2202-9

890

891 Yang, Q., Ma, Z., and Xu, B.: Modulation of monthly precipitation patterns over East China by the
892 Pacific Decadal Oscillation, Climatic change, 144, 405-417, 2017. DOI: 10.1007/s10584-016-1662-
893 9

894

895 Yatagai, A., Kamiguchi, K., Arakawa, O., Hamada, A., Yasutomi, N., and Kitoh, A.: APHRODITE;
896 Constructing a long-term daily gridded precipitation dataset for Asia based on a dense network of
897 rain gauges, Bulletin of the American Meteorological Society, 93(9), 1401-1415, 2012.
898 https://doi.org/10.1175/BAMS-D-11-00122.1

899

900 Yin, J., and Zhang, Y.: Decadal changes of East Asian jet streams and their relationship with the
901 mid-high latitude circulations, Climate Dynamics, 56, 2801-2821, 2021.
902 https://doi.org/10.1007/s00382-020-05613-8

903

904 Yuan, X., Yang, K., Lu, H., He, J., Sun, J., and Wang, Y.: Characterizing the features of precipitation
905 for the Tibetan Plateau among four gridded datasets: Detection accuracy and spatio-temporal
906 variabilities, Atmospheric Research, 264, 105875, 2021.
907 https://doi.org/10.1016/j.atmosres.2021.105875

908

909 Zhang, Y., Wallace, J. M., and Battisti, D. S.: ENSO-like interdecadal variability: 1900–93, Journal
910 of climate, 10(5), 1004-1020, 1997. https://doi.org/10.1175/1520-0442(1997)010%3C1004:ELIV
911 %3E2.0.CO;2

912

913 Zhang, R., and Delworth, T. L.: Impact of the Atlantic multidecadal oscillation on North Pacific
914 climate variability, Geophysical Research Letters, 34(23), 2007.
915 https://doi.org/10.1029/2007GL031601